# Effect of density on tensile strength, fracture toughness, and fatigue crack propagation behaviour of sintered steel

N. A. Fleck and R. A. Smith

The tensile strength, fatigue crack propagation behaviour, and fracture toughness of a low-alloy sintered steel were determined for the porosity range 11–17%. Static and cyclic strength were found to increase with density in a non-linear fashion. The pores both exerted a stress-concentrating influence and reduced the load-bearing section. The micromechanism of failure was always ductile fracture in the necks between sintered steel particles. It was concluded that the stress state at the tips of cracks subjected to static or cyclic loading was closer to plane stress than to plane strain. Retardation of fatigue crack propagation appeared to occur due to the blunting action of the pores. The presence of a wear mechanism had little influence upon fatigue crack growth rates. A companion paper (following) attempts to model the static and cyclic behaviour of the steel, based on the known micromechanisms of failure. PM/0172

 Manuscript received 30 October 1980; in final form 1 April 1981. The authors are in the Engineering Department, University of Cambridge.

In recent years sintered steels have been developed for mass produced components which are subjected to large mechanical stresses. It is therefore necessary to determine the static and cyclic strength of such materials.

The distinguishing feature of sintered materials is their porosity. Often the porosity has a dominating influence upon the mechanical properties of the material. It is generally found that an increase in density leads to an increase in tensile strength, fracture toughness, and resistance to fatigue crack growth. Sintered steels therefore possess the property that fracture toughness increases with tensile strength,[1,2] unlike the behaviour of fully dense steels.

To investigate the relationship between density, tensile strength, fatigue crack propagation behaviour, and fracture toughness, the micromechanisms of failure of a sintered steel were studied. A companion paper[3] contains a theoretical model for the behaviour of the sintered steel based on the results given in this paper.

## PREPARATION OF TESTPIECES

A Höganäs diffusion alloyed powder of type Distaloy SA was used. It had a composition of Fe–1·75Ni–1·50Cu–0·50Mo–0·50C and was derived from sponge reduced ore. Particle size varied from less than 44 to 230 $\mu$m (*see* Table 1).

Two different types of testpiece were compacted and sintered: tensile testpieces of 'dog-bone' geometry, and three-point bend specimens (Fig. 1). The bend specimens were used for investigating fatigue and fracture-toughness behaviour.

Compaction pressure was varied to give three different as-sintered densities for each testpiece, as summarized in Table 2. Sintering of the two types of specimen was carried out simultaneously, for 30 min at 1150°C in an atmosphere of cracked ammonia.

## EXPERIMENTAL PROCEDURE

Five tensile testpieces of the three densities were strain gauged and then pulled to failure. The 0·2% offset yield stress and the ultimate tensile stress were noted.

Fatigue crack propagation rates were determined for three bend specimens of each density, on application of loads in the range 5·0–11·0 kN, at 500 cycles min$^{-1}$. The tip of the 5 mm machined notch was manually sharpened to aid fatigue crack initiation. Crack propagation rates were determined using a cycle counter and a travelling microscope.

Fracture toughness tests were carried out on the three-point bend specimens in accordance with the standard procedure ASTM E399–78.[5]

A tensile specimen of each density was sectioned and examined using an optical microscope. Pore morphology and particle microstructure were thus observed. The fracture surfaces of tensile testpieces, bend specimens subjected to fatigue loading, and bend specimens subjected to the fracture-toughness rising force test were examined using a scanning electron microscope. This provided evidence for determining the micromechanisms of failure under static and cyclic loading.

## RESULTS: METALLOGRAPHY AND FRACTOGRAPHY

### Metallography

As the specimen density was increased from 6550 to 6980

**Table 1 Sieve analysis of diffusion alloyed powder**

| Size range, $\mu$m | Fraction, wt-% |
|---|---|
| 149–230 | 2 |
| 44–149 | 78 |
| Less than 44 | 20 |

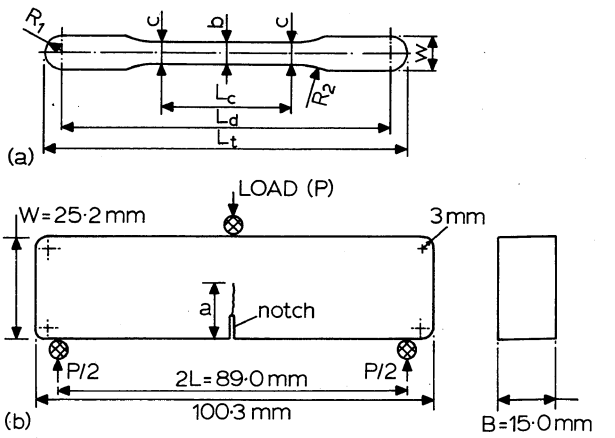


*a* tensile testpiece, values (mm): $b=5{\cdot}70\pm0{\cdot}02$, $c=b+0{\cdot}25$, $L_c=32$, $L_d=81{\cdot}0\pm0{\cdot}5$, $L_t=89{\cdot}7\pm0{\cdot}5$, $w=8{\cdot}7\pm0{\cdot}2$, $R_1=4{\cdot}35$, $R_2=25$; *b* three-point bend specimen: $K=3PL/BW^{3/2}=[1{\cdot}93\,(a/W)^{1/2}-3{\cdot}07\,(a/W)^{3/2}+14{\cdot}53\,(a/W)^{5/2}-25{\cdot}11\,(a/W)^{7/2}+25{\cdot}80\,(a/W)^{9/3}]$

**1 Geometry of testpieces: tensile testpiece in accordance with standard ISO 2740–1973 (E),[4] bend specimen in accordance with standard ASTM E399–78[5]**

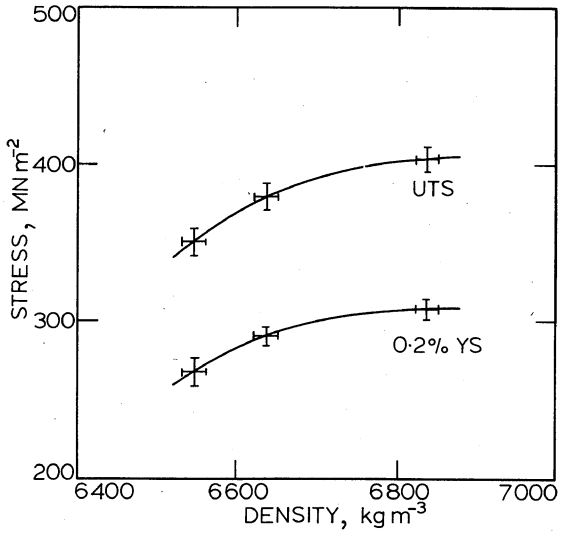


**2 Effect of density on ultimate tensile stress (UTS) and yield stress (0·2% YS)**

kg $m^{-3}$, it was found that the average pore size decreased, the number of pores per unit area increased slightly, and the pores became less interconnected and less acute in shape. The pores were filmlike in character, surrounding much of the sintered steel particles. The microstructure was very inhomogeneous, consisting of a mixture of martensite, upper bainite, pearlite, and ferrite within each particle.

### Yield stress and ultimate tensile stress

The average yield stress and ultimate tensile stress at each density were found to increase with density as shown in Fig. 2. On examination of the fracture surfaces with a scanning electron microscope it was apparent that fracture was due to microvoid coalescence in the necks between adjoining steel particles (Fig. 3). Some microvoids pre-existed in the material; others nucleated and grew from defects such as inclusions.

### Fatigue crack propagation behaviour

From observations of fatigue crack length and number of cycles, logarithmic plots of crack growth rate $da/dN$, against stress-intensity factor range $\Delta K$, were determined for the three densities of sintered steel (*see* Fig. 4). Each data point represents the average for the three specimens tested at each density. The straight lines are least-squares fits.

Crack growth rates were recorded for only a small range of $\Delta K$ from 10 to 17 MN $m^{-3/2}$. This was because the threshold $\Delta K_{th}$ for the material was 5–7 MN $m^{-3/2}$ while the plane-strain fracture toughness was approximately 20 MN $m^{-3/2}$. From Fig. 4, the linear Paris law

$$da/dN=10^{-9}.(\Delta K/\Delta K_0)^m \text{ m/cycle}$$

is obeyed for the material. The term $\Delta K_0$ refers to the stress-intensity factor range corresponding to a growth rate of $10^{-9}$ m/cycle. The variation of $m$ and $\Delta K_0$ with density is given in Table 3.

Scanning electron microscopy showed that cracks advanced largely by the process of microvoid coalescence in the necks between sintered steel particles. Again, microvoids nucleated and grew from microstructural defects and resulted in the ductile-type fracture. The necks appeared to fail by three distinct mechanisms, as observed by other workers:[6–8]

(i) a cyclic ductile fracture mechanism, whereby the crack advanced by a process of microvoid coalescence (*see* Fig. 5*a*). This mechanism operated even when observed crack growth rates were less than the typical inclusion spacing.[9] For $\Delta K$ less than 10 MN $m^{-3/2}$, plastic tearing also took place, resulting in

**Table 2 Density of tensile and three-point bend testpieces**

| Testpiece type | Sintered density, kg $m^{-3}$ | Theoretical density, % |
|---|---|---|
| Tensile | 6550 | 83·4 |
| | 6640 | 84·6 |
| | 6840 | 87·1 |
| Bend specimens | 6580 | 83·8 |
| | 6810 | 86·8 |
| | 6980 | 88·9 |

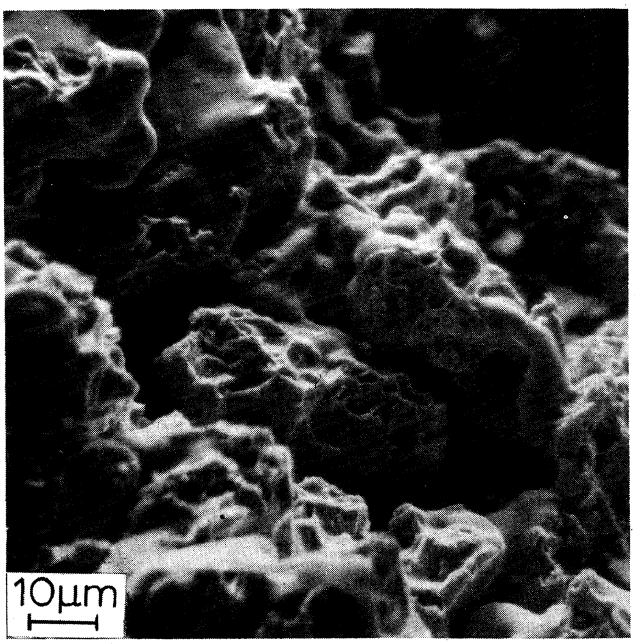


**3 Fracture surface of tensile testpiece: $\rho$=6640 kg $m^{-3}$**

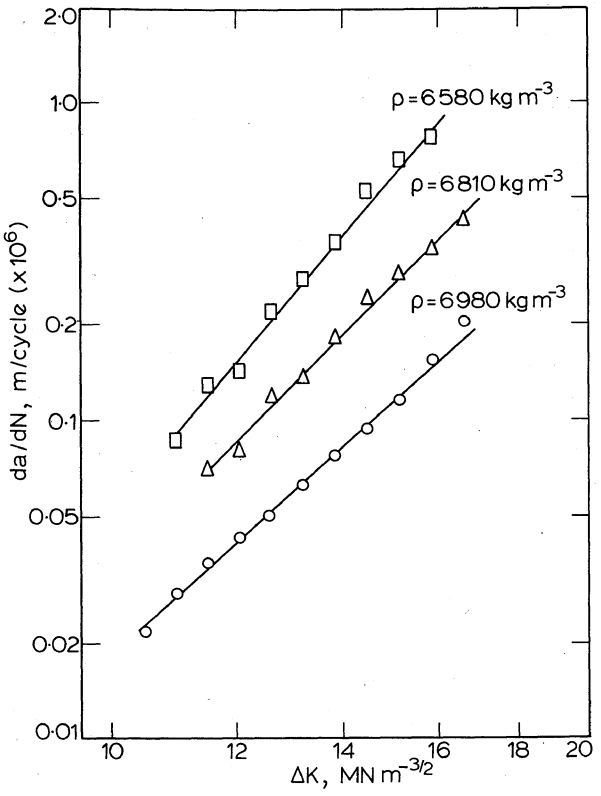


**4 Effect of density on fatigue crack propagation behaviour**

striation formation. Typical striations are shown in Fig. 5*b–d*. Similar observations were reported by Rodziňák and Šlesár:[8] they found most striations on those specimens subjected to the smallest cyclic stresses

(ii) static shear failure, where the local shear stress approached the yield shear stress. This type of fracture occurred where the crack front came upon an unfavourably oriented particle (*see* Fig. 5*b*)

(iii) static ductile fracture, where the neck ligament was unable to support the applied load (Fig. 5*b*).

In all three cases failure was nucleated at inclusions, voids, and other microstructural defects within the necks. Microvoids grew and coalesced from these defects until fracture took place.

### Fracture-toughness tests

Fracture-toughness values were determined using the standard ASTM E339–78[5] calibration equation for the single edge notch geometry (Fig. 1). The variation in fracture toughness $K_C$ with density is shown in Fig. 6. Fracture toughness increased from 22 to 26 MN m$^{-3/2}$ as the density was increased from 6580 to 6980 kg m$^{-3}$. Microscopic examination of the fracture surfaces showed that failure had again resulted from the coalescence of microvoids in the necks of the sintered steel particles; a typical fracture surface is shown in Fig. 7.

## DISCUSSION

### Tensile behaviour

It is seen from Fig. 2 that both the yield stress (YS) and ultimate tensile stress (UTS) increase non-linearly with density. The filmlike porosity gives rise to both a reduction in load-bearing section and a stress concentration effect; these pores obviously reduce the tensile strength of the material.

**Table 3 Effect of density on Paris law constants *m* and $\Delta K_0$***

| Density, kg m$^{-3}$ | Paris law index *m* | $\Delta K_0$, MN m$^{-3/2}$ |
|---|---|---|
| 6580 | 5·7 | 4·9 |
| 6810 | 5·0 | 4·9 |
| 6980 | 4·5 | 5·2 |

*$da/dN = 10^{-9}\ (\Delta K/\Delta K_0)^m$ m/cycle; *m* is the Paris law index; $\Delta K_0$ corresponds to a growth rate of $10^{-9}$ m/cycle.

### Fatigue behaviour

Consideration of Table 3 and Fig. 4 leads to the conclusion that fatigue crack propagation rates increase rapidly with an increase in $\Delta K$ and a decrease in density. The Paris law index *m* decreased from 5·7 to 4·5 as the density of sintered steel was increased from 6580 to 6980 kg m$^{-3}$. One reason for this is that the maximum stress-intensity factor $K_{max}$ associated with each fatigue cycle was not much less than the fracture toughness of the material; the load ratio (=minimum load/maximum load) was set at the high value of 0·45. Significant static tearing therefore occurred in addition to fatigue crack advance. This would have the effect of increasing the apparent value for *m*. A comparison of Fig. 4 with fatigue crack propagation data on fully dense steels[10] shows that cracks propagate an order of magnitude faster through sintered steels than through a fully dense steel of similar tensile properties, for $\Delta K$ in the range 10 to 17 MN m$^{-3/2}$.

The fractographs (Fig. 5*a–c*) clearly show that a crack grows by following the filmlike pore structure through the specimen, cutting through the interparticle necks on its way. Table 4 and Fig. 8 summarize the typical conditions prevailing at the tip of the growing fatigue crack. Since the cracking mechanism is one of the necks failing like microtensile specimens it appears reasonable to follow the argument of Ingelström and Ustimenko[11] and assume that the stress state at the crack tip is closer to plane stress than to plane strain. Plane-stress equations are therefore considered in Table 4. This relaxation of hydrostatic stress across the thickness of the specimen encourages a ductile type of fracture under both static and cyclic conditions. No sign of cleavage is apparent on the fracture surfaces of tensile testpieces or bend specimens.

We can draw a number of conclusions from Table 4 and Fig. 8:

(i) since the reversed plastic zone size $2r_y$ is greater than the average particle size, we can use quasilinear elastic fracture mechanics. Barnby *et al.*[2] found that the calculated plastic zone size agreed with their measured value and came to a similar conclusion

(ii) the calculated radius of curvature *r*, at the tip of the growing fatigue crack appears to be an order of magnitude smaller than the measured local radius of curvature *R*, at the necks. We may therefore expect the pores to blunt the crack tip and so retard fatigue crack propagation rates. This retardation process has also been suggested by Williams and Haynes.[7] Their work on sintered nickel suggests that the fatigue crack tip is continually being reformed at the leading edge of the pores. Crack-tip blunting can also be inferred from the work of Wheatley and Smith.[12] They found that the stress-concentrating effects of the pores were negligible in comparison with the stress-concentrating effects of the fatigue crack. However, since fatigue cracks propagate an

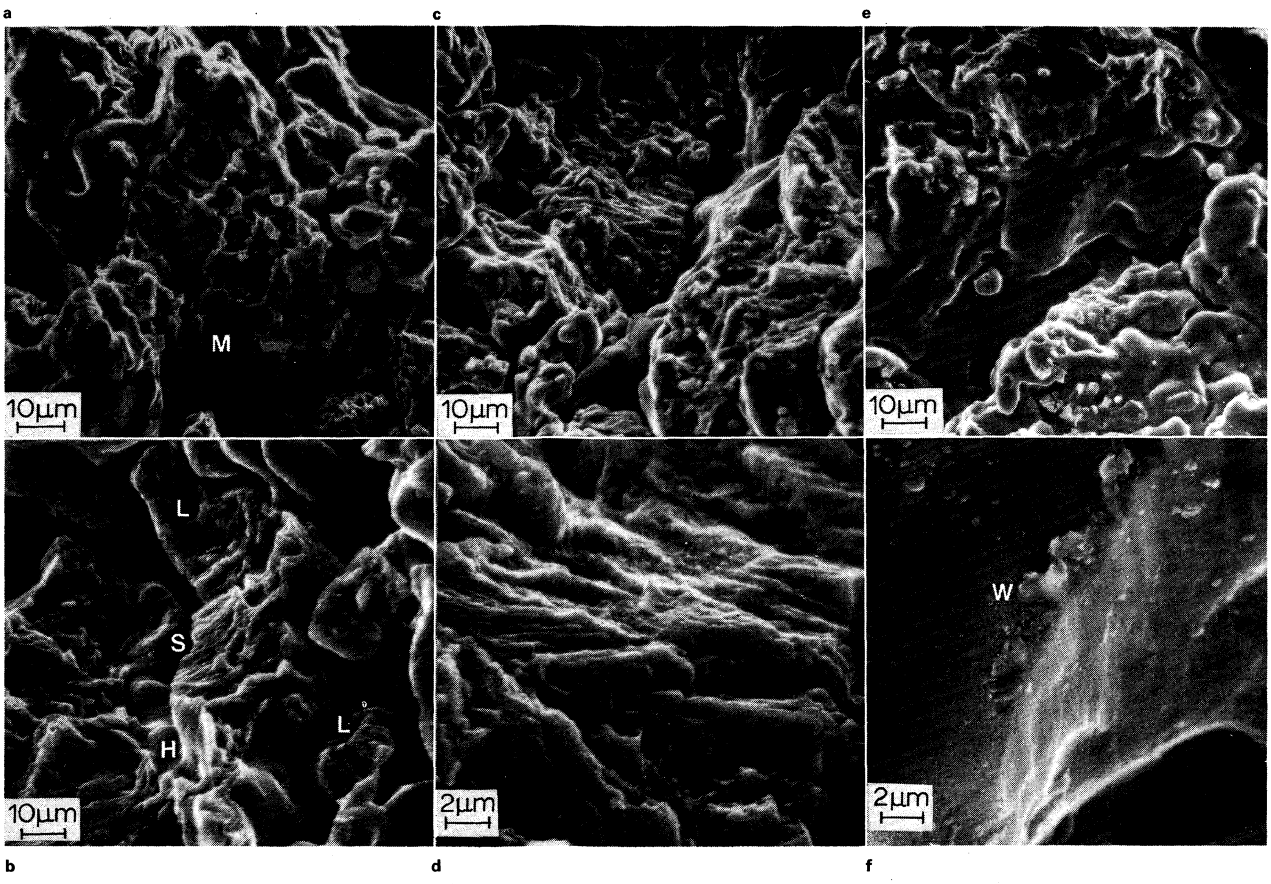


*a* $\Delta K$=14 MN m$^{-3/2}$; *b* $\Delta K$=8 MN m$^{-3/2}$; *c, d* $\Delta K$=8 MN m$^{-3/2}$; *e, f* $\Delta K$=14 MN m$^{-3/2}$

**5 Fracture surface of fatigued bend specimen: *a, b* $\rho$=6810 kg m$^{-3}$; M=crack advance by microvoid coalescence, S=striations, H=static shear failure, L=ligament failure by microvoid coalescence; *c* and *d* show striations, same region appears in both micrographs, $\rho$=6810 kg m$^{-3}$; *e, f* show wear region, same part of surface shown in both micrographs, $\rho$=6810 kg m$^{-3}$, W=wear debris**

order of magnitude faster through sintered steel than the fully dense material, it is concluded that crack blunting effects are much less significant than the reduction in load-bearing area due to the pores.

Examination of the fracture surfaces of the bend specimens shows that an adhesive wear mechanism operates alongside fatigue crack advance (Fig. 5*e, f*). What form does this mechanism take? Consider a particle which is attached to the top surface of the fatigue crack, having undergone shear failure from particles of the bottom surface of the fatigue crack. Under the applied cyclic loads, this particle rubs against its neighbours from the bottom surface of the crack, producing wear debris. Typical wear debris is shown in Fig. 5*f*. The mechanism probably operates just behind the crack tip, where the fracture surfaces are still close together. Since the worn regions occupy only 0·01% of the fracture surface,

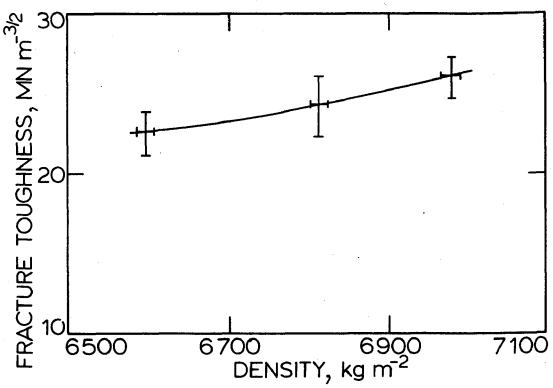


**6 Effect of density on fracture toughness**

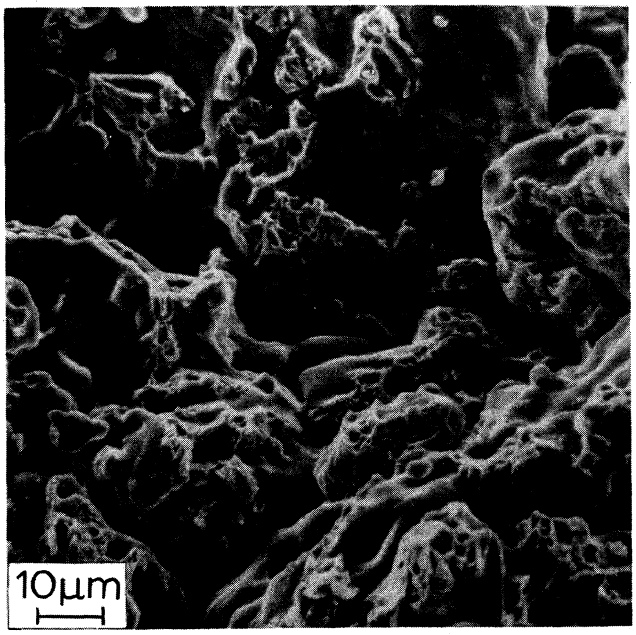


**7 Fracture surface of fracture-toughness specimen: $\rho$=6810 kg m$^{-3}$**

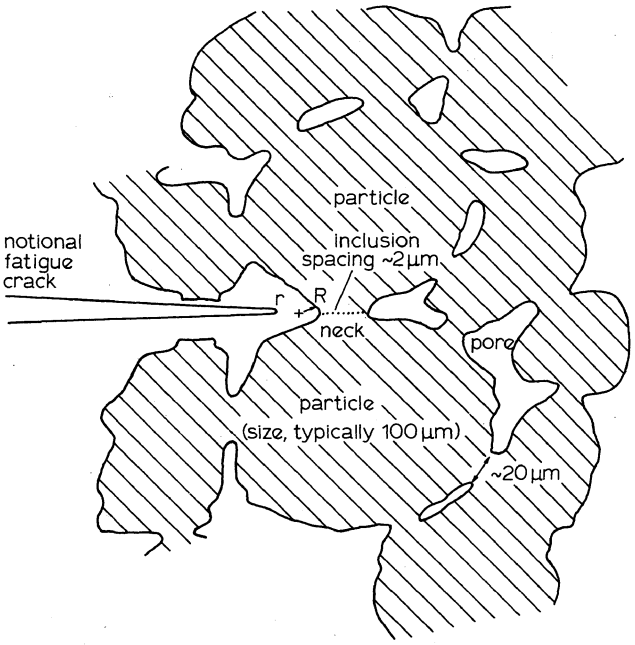


**8 Conditions at tip of propagating fatigue crack: size of reversed plastic zone at crack tip ~150 μm, crack-tip radius $r$ ~0·7 μm, radius of curvature at binding necks $R$ ~10μm**

it is concluded that the wear mechanism has an insignificant effect on fatigue crack growth rates.

### Fracture-toughness behaviour

Fracture toughness is seen to increase disproportionately with density (Fig. 6). Strictly, none of the tests are valid plane-strain fracture-toughness tests because the crack length $a$ and specimen thickness $B$ are less than the ASTM thickness criterion, $2{\cdot}5\ (K_C/\sigma_y)^2$. We can argue that the tests are a useful measure of fracture toughness, however, for the following reasons:

(i) on a macroscopic level, the fracture surfaces appear to be of the 'flat plane strain type'; no shear lips are formed

(ii) since failure occurs at the necks of the sintered steel particles, where the hydrostatic/shear stress ratio is reduced, the stress state at the crack tip is closer to plane stress than to plane strain.[11]

It is deduced that the measured fracture toughness of sintered steel varies to a smaller degree with specimen size than for the fully dense material. Convincing experimental evidence for this is shown in the associated paper.[3]

The crack-tip radius $r$ at incipient static failure is compared with the local radius of curvature $R$ at the necks in Table 5. It appears that the two radii are comparable in magnitude: the pores neither sharpen nor blunt the advancing crack. This accounts for the experimental findings of Barnby *et al.*[2] that fatigue cracking is an unnecessary precursor to the fracture-toughness testing of sintered steel; a notch of root radius about 0·1 mm, e.g. produced by a saw blade, is sufficient. This has serious implications for the design of sintered steel components: any notch inherently possesses a sharp root by virtue of the small radius of curvature $R$ at the necks. Thus more attention should be paid to the fatigue and fracture aspects of sintered steel component design.

**Table 4 Typical conditions at fatigue crack tip**

| Feature | Equation | Size, μm |
|---|---|---|
| Reversed plastic zone size $2r_y$ | $2r_y \simeq 1/4\pi(\Delta K/\sigma_y)^2$ | ~150 |
| Radius of curvature $R$, at necks | .. | ~10 |
| Radius of curvature $r$, at tip of fatigue crack | $r \simeq \Delta K^2/4E\sigma_y$ | ~0·7 |
| Typical spacing of coalesced microvoids in failed necks | .. | ~2 |

**Table 5 Comparison of crack-tip radius $r$ at incipient static failure with local radius of curvature $R$, at binding necks**

| Feature | Equation | Size, μm |
|---|---|---|
| Radius of curvature $R$, at necks | .. | ~10 |
| Crack tip radius $r$, at incipient unstable crack propagation | $r \simeq K^2/2E\sigma_y$ | ~4 |

## CONCLUSIONS

The yield stress, ultimate tensile stress, resistance to fatigue crack propagation, and fracture toughness of sintered steel depend critically upon the density. Close production control must therefore be exercised if sintered steel components are to show little scatter in static and cyclic life.

The micromechanisms of fracture in uniaxial tensile failure, fatigue failure, and failure due to the unstable propagation of a crack are all identical. This micromechanism is one of ductile fracture by microvoid coalescence in the necks of the sintered steel particles. From a knowledge of the micromechanisms of fracture and the tensile properties possessed by the sintered steel, it should be possible to model its static and cyclic fracture behaviour. A companion paper[3] attempts to develop such models.

## ACKNOWLEDGMENTS

One of the authors (NAF) is supported by a research studentship from the Department of Education, Northern Ireland. Both authors thank GKN Group Technological Centre for providing the testpieces.

## REFERENCES

1. W. S. PELLINI: National Research Laboratory Report, 7406, 1972.
2. J. T. BARNBY, D. C. GHOSH, and K. DINSDALE: *Powder Metall.*, 1973, **16**, (31), 55.
3. N. A. FLECK and R. A. SMITH: *ibid.*, this issue, 126–130.
4. International Standard ISO 2740, 1973 (E), 'Sintered metal materials (excluding hardmetal) – tensile test pieces', (1 ed.), 1973–12–01.
5. 'Standard test method for plane-strain fracture toughness of metallic materials', ASTM Standards, E399–78, 1978, 512.
6. P. FRANKLIN and B. L. DAVIES: *Powder Metall.*, 1978, **21**, 7.
7. S. H. WILLIAMS and R. HAYNES: *ibid.*, 1973, **16**, (32), 387.
8. D. RODZIŇÁK and M. ŠLESÁR: *Powder Metall. Int.*, 1980, **12**, (3), 127.
9. M. F. ASHBY: 'Fracture mechanics – current status, future prospects', (ed. R. A. Smith), 1; 1980, Oxford, Pergamon.
10. L. P. POOK and R. A. SMITH: 'Fracture mechanics – current status, future prospects', (ed. R. A. Smith), 29; 1980, Oxford, Pergamon.
11. N. INGELSTRÖM and V. USTIMENKO: *Powder Metall.*, 1975, **18**, (36), 303.
12. J. M. WHEATLEY and G. C. SMITH: *ibid.*, 1963, **6**, (12), 141.